AD-A090 421 ARMY ARMAMENT RESEARCH AND DEVELOPMENT COMMAND ABERD--ETC F/G 19/4
ARMOR DESIGN BASED ON MATERIAL PROPERTIES,(U)
JUN 80 G L MOSS

UNCLASSIFIED NL

1 OF 1
AD A 090421

END
DATE FILMED
11-80
DTIC

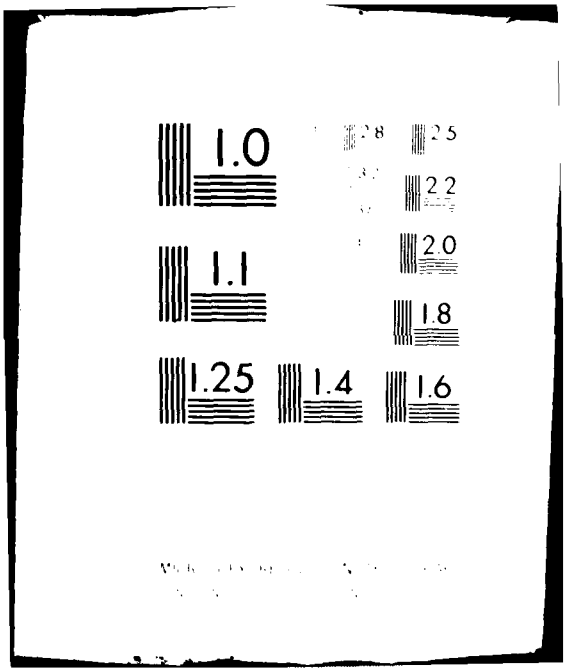
1.0
2.8
2.5
2.2
1.1
2.0
1.8
1.25
1.4
1.6

ARMOR DESIGN BASED ON MATERIAL PROPERTIES (U)

JUN 1980

GERALD L. MOSS, PhD
USA ARRADCOM, BALLISTIC RESEARCH LABORATORY
ABERDEEN PROVING GROUND, MARYLAND 21005

I. INTRODUCTION

As a result of extensive research over the last 20 years, an analysis of high-rate loading and fracture has evolved that models the three main features of failure caused by stress waves. The nucleation and growth of voids are the governing processes on which the model is based. In the following, a description will be given of the characterization of a rolled homogeneous steel armor and a penetrator alloy in terms of this model. It will be shown by the results that the model is sensitive to the microstructural detail of the materials characterized. Finally, extensions of the model that are essential to the design of armor will be described along with an indication of how such a design is accomplished.

II. FRACTURE WITH STRESS WAVES

The nucleation, growth and coalescence of large numbers of voids were first identified as characteristic features of fracture with stress waves (spallation) in 1960.(1,2) Large numbers of independent voids are a unique feature of spallation and occur because stresses much greater than the strength of a material can be applied before there is appreciable crack growth. This is possible because crack velocities cannot exceed approximately $0.38\sqrt{E/\rho}$ ($\sqrt{E/\rho}$ is the longitudinal elastic wave velocity V_1), and because disturbances associated with the opening of a void can only be transferred with the speed of stress waves. A high density of independent voids is, therefore, a general feature of spallation.

Seaman, Barbee, Crewdson, and Curran subsequently developed an ingeneous technique that allows one to describe the spallation of a given material quantitatively.(3,4) The technique is based on an experimental determination of an expression that characterizes the size distribution N(R) (R is the radius of the void) of voids and rate equations, $\dot{N}$ and $\dot{R}$, for the nucleation and growth of voids. No assumption is made about the form of these equations. It is only assumed that the progression of failure can be described in terms of these variables.

The approach is to determine the relations for N(R), $\dot{N}$ and $\dot{R}$ experimentally with plate impact tests conducted over a range of impact velocities. Details of the method have been described in summary articles,(4,5) but it is emphasized that a unique and especially important feature of the analysis is the method of handling large numbers of voids. This has been possible through a continuum approach that describes void densities, N(R), at a point. Another unique feature of the model is that it includes a description of the effect of fracture on the loading history. It is, therefore, a truly "active" fracture model.

Characterizations of the spallation of several materials,(6) including Al, Cu, Fe, S-200 Be and Lexan have resulted in expressions for N(R), $\dot{N}$ and $\dot{R}$, and it has been found that equations with the same form approximate the behavior of each of these materials. These equations are

$$N(R) = N_o e^{-R/R_1} \tag{1}$$

$$\dot{N} = \dot{N}_o e^{(\sigma-\sigma_{no})/\sigma_1} \tag{2}$$

$$\dot{R} = (\sigma-\sigma_{go})R/4\eta \ . \tag{3}$$

The parameters N_o, R_1, $\dot{N}_o$, σ_{no}, σ_1, σ_{go}, and η reflect the nature of a material, and the rate equations depend on the applied stress σ explicitly which makes the progression of failure sensitive to the loading history. Once the Eqs. for N, $\dot{N}$ and $\dot{R}$ have been determined for a specific material, the approximate spallation of this material can be predicted for general stress histories bounded by the range of the calibration. Presumably, the range of applicability can be extended somewhat by an extrapolation of results.

III. SPALLATION OF STEEL ARMOR

In a characterization of the spallation of a low alloy Ni-Cr

rolled steel armor (RHA) with the approach just described, it was found that Eqs. 1-3 are also approximately representative of the spallation behavior of this material. The material parameters determined are listed in Table I along with similar results for a W-7Ni-3Fe penetrator alloy and Cu.(6) The parameters for each of the materials are different as they should be in a realistic material-dependent model, but even though they are different for each material and allow one to compute how a previously characterized material will break under general loading conditions, it is still not possible to design materials with the nucleation and growth (NAG) model. This possibility has

TABLE I

VOID NUCLEATION AND GROWTH PARAMETERS FOR SPALLATION

PARAMETER	UNITS	RHA*	90W-7Ni-3Fe	Cu
σ_{no}	GPa/cm^2	1.8	-2.8	-0.50
$\dot{N}_o$	$No/(cm^3 sec)$	5.0×10^8	2.5×10^{14}	2.8×10^{12}
σ_1	GPa/cm^2	-0.25	-2.53	-0.20
σ_{go}	GPa/cm^2	-0.2	-1.0	-0.50
$1/4\ \eta$	$cm^2/(GPa\ sec)$	-7.0×10^5	-5.0×10^6	-1.3×10^7
R_1	cm	3.0×10^{-3}	1.4×10^{-4}	1.0×10^{-4}

*1.27cm rolled steel armor plate

eluded us because of the order in which we have learned about spallation. Initially, the goal was to quantitatively describe N(R), $\dot{N}$ and $\dot{R}$ with simple enough equations to be useful in treating complex ballistics problems. The approach was to use the data from plate impact-fracture tests exclusively to establish the equations.(4) Hence, the equations certainly apply to spallation, but the parameters are not necessarily related to material variables that are known to govern mechanical behavior and to be controllable with manufacturing methods. These connections still need to be made.

Apparently, more information is required about the NAG parameters and material behavior before material design can be attempted with the nucleation and growth equations. Some information

(5.27

along these lines is implied by the crack-size distributions that were used in determining the parameters listed in Table I. A typical result is shown in Fig. 1 where it can be seen how the cumulative number of cracks varied with crack radius. Clearly, these results cannot be completely described with Eq. 1, although it is made up of straight-line segments.

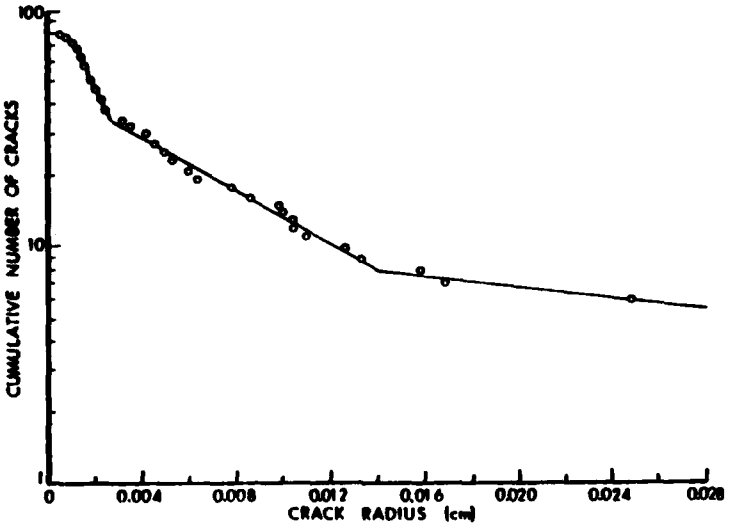

Figure 1. Size distribution of cracks formed in steel armor (1.27cm RHA) with the stress waves from a plate impact. Impact velocity was 0.1178 mm/μsec.

Without additional information, it is not obvious why the curve is segmented, but when the cracks were observed on cross sections of partially broken samples, the reasons for the two changes in slope became clear. Three distinct stages of cracking were observed, and these are illustrated with Figs. 2 through 4.

First, there was crack nucleation at MnS inclusions during which the inclusions were cracked as well as separated from the matrix. At intermediate stages of cracking, short irregularly oriented "hair-line" cracks extended from inclusion to inclusion in planes approximately parallel to the plane of the plate. Most of the MnS inclusions were found in these planes which were the weak planes of a banded microstructure that is typical of rolled steel armor. In the last stage of failure, long non-coplanar cracks opened and coalesced by plastic shear on connecting surfaces.

5.31

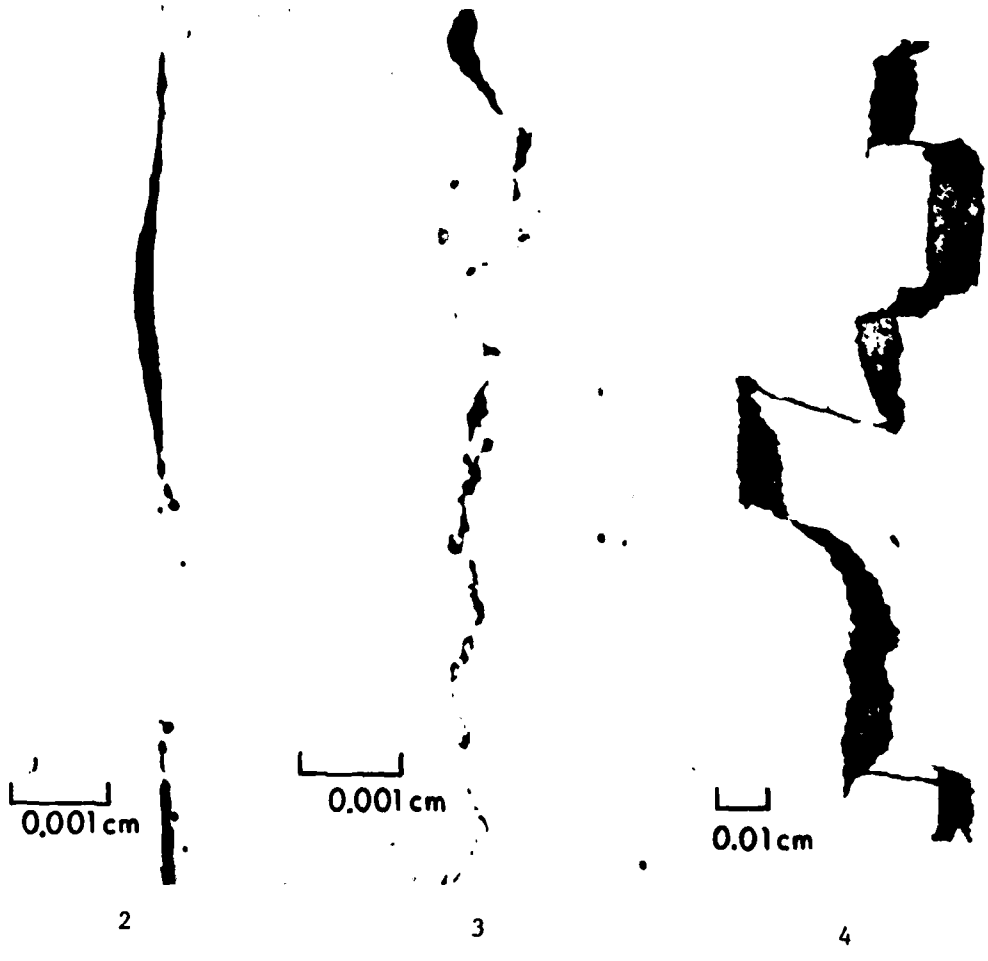

Figure 2. Early stage of fracture in steel armor showing crack nucleation at sulfide inclusions.

Figure 3. Intermediate stage of fracture in steel armor showing cracks extending from inclusion to inclusion in approximately a single plane.

Figure 4. Late stage of fracture of steel armor showing the coalescense of non-coplanar cracks by plastic shear on connecting surfaces.

(531)

These distinct stages of cracking are exactly what is reflected in the crack-size distribution shown in Fig. 1. The part of the curve bounded by $R \leq 0.0025$cm is the region where there was primarily nucleation at MnS inclusions. Inclusion diameters observed with the optical microscope ranged from the resolution limit to 0.005cm. The change in slope at 0.0025cm corresponds to the beginning of the intermediate stage of cracking. Finally, the change in slope at $R = 0.0135$cm is an indication of the onset of coalescence of non-coplanar cracks. This is in agreement with the crack lengths in Fig. 4 which range from 0.01 to 0.04cm.

The coalescence of the non-coplanar cracks is the mechanism by which the material finally comes apart, and an independent model of this phenomenon has been presented by Seaman et al.(5) Hence, the consideration will be limited here to the first two stages of failure. These can be reasonably approximated with the NAG analysis because the volume of the cracks with radii less than 0.0025cm is small compared with the total crack volume. They contribute little to the total separation, and it is sufficient to describe the size distribution of cracks with radii in the range $0.0025 \leq R \leq 0.0135$cm. Hence, even though the entire curve in Fig. 1 is too complex to be described with Eqs. 1-3, they reasonably approximate the intermediate stage of cracking. This is the important stage to characterize because this is when the greatest void volume, i.e., damage, develops.

An important conclusion to be drawn from these observations is that the crack measurements displayed in Fig. 1 are sensitive to the microstructure of the material. Clearly, banding, inclusion size and inclusion distribution are important microstructural features that govern the failure of RHA, and if a method were to be derived to allow steel armor to be tailored to resist spallation, it would be important to include the effects of banding and inclusions in the analysis. Such an analysis will be presented next.

IV. MATERIAL DEPENDENCE OF FRACTURE

Conceivably, the material dependence of the parameters in Eq. 3 could be established by deriving an independent relation for $\dot{R}$ in terms of the governing material features and equating it to Eq. 3. Such an attempt will be described because it has yielded useful results.

The velocity of an elastic crack $\dot{C}_e$ can be determined from an expression of energy conservation during fracture

(532)

$$\frac{d}{dC}\left(-\frac{\pi\sigma^2C^2}{E} + 4\gamma C + \tfrac{1}{2}k\rho\dot{C}_e^2C^2\frac{\sigma^2}{E^2}\right) = 0, \qquad (4)$$

where the first term in parenthesis is the elastic energy, the second term is the surface energy and the last term is the kinetic energy. The applied stress is σ, C is the crack radius, γ is the surface energy, ρ is the material density and E is Young's modulus.

Differentiating Eq. 4 and solving for $\dot{C}_e^2$ leaves

$$\dot{C}_e^2 = \left(\frac{2\pi\sigma^2C}{E} - 4\gamma\right)\left(\frac{1}{k\rho C}\right)\left(\frac{E}{\sigma}\right)^2. \qquad (5)$$

This can be expressed in terms of the critical crack size C_o at which crack growth becomes unstable. This is given by the Griffith condition as

$$C_o = \frac{2\gamma E}{\pi\sigma_c^2}, \qquad (6)$$

where σ_c is the critical stress corresponding to the instability condition. Substituting Eq. 6 into Eq. 5 and solving for $\dot{C}_e$ leaves

$$\dot{C}_e = \sqrt{\frac{2\pi}{k}}\sqrt{\frac{E}{\rho}}\left(1 - \frac{C_o\sigma_c^2}{C\sigma^2}\right)^{\frac{1}{2}}. \qquad (7)$$

Usually, stresses are applied gradually until σ equals σ_c, and it is assumed that subsequent failure proceeds at this stress level. Then,

$$\dot{C}_e = \sqrt{\frac{2\pi}{k}}\,V_1\left(1 - \frac{C_o}{C}\right)^{\frac{1}{2}}. \qquad (8)$$

This is the equation commonly used for $\dot{C}_e$. However, as explained in §2, it is possible to impose stresses during fracture that are much greater than σ_c when the loads are applied with stress waves. Then, Eq. 7 is the correct expression for $\dot{C}_e$.

Steel armor is not a purely elastic material, but also deforms plastically as it fails. It is well known that for such materials, the expression for the surface energy should include the effects of plastic deformation. Gilman(7) has described such a result, and if it is combined with his relation for the surface energy of elastic cleavage, an expression is obtained for the energy of a

533

cleaved surface formed with plastic deformation. The result is

$$\sigma_p = \frac{9E_{hkl}}{y_{hkl}} \left(\frac{a_o}{\pi}\right)^2 \ln\left(\frac{2G}{\pi\sigma_Y}\right) , \qquad (9)$$

where the indeces hkl define the cleavage plane, y_{hkl} is the distance between cleavage planes, a_o is the atomic radius, G is the shear modulus and σ_Y is the yield strength.

There is an additional plastic effect on the crack velocity that has previously been ignored. The effect is to shift the elastic stress field beyond the crack by the range of the plastic strain field. For plane-strain conditions, applicable when loading is with one-dimensional stress waves, the length of the plastic zone in front of the crack tip is given by(8)

$$R_m = \rho_t \left[e^{(\pi-\alpha)/2} - 1\right] , \qquad (10)$$

where ρ_t is the crack-tip radius, and α is the wedge angle of the crack.

The factor $\sqrt{2\pi/k}$ in Eq. 7 equals the range of the stress field(7) normalized to the crack length. It is limited to $\dot{C}_m/V_1$ ($\dot{C}_m$ is the maximum crack velocity) for an elastic material, but when there is plastic deformation, this must be increased by R_m/C. Hence, when there is a plastic zone leading the crack,

$$\sqrt{\frac{2\pi}{k}} = \frac{\rho_t\left[e^{(\pi-\alpha)/2} - 1\right]}{C} + \frac{\dot{C}_m}{V_1} . \qquad (11)$$

The radius of the crack tip is approximately $\rho_t = C\sigma^2/(2\sigma_Y G)$.(7,9)

Substituting Eq. 11 for $\sqrt{2\pi/k}$ and Eq. 9 for γ in Eq. 7, indicates that the crack velocity $\dot{C}_p$ in an elastic-plastic material is given by

$$\dot{C}_p = \left\{\frac{\sigma^2}{2\sigma_Y G}\left[e^{(\pi-\alpha)/2} - 1\right] + \frac{\dot{C}_m}{V_1}\right\} V_1 \left\{1 - \frac{\frac{\sigma_c^2}{\sigma_Y^2}\frac{18}{\pi}E_{hkl}\left[\frac{E_{hkl}}{Y_{hkl}}\left(\frac{a_o}{\pi}\right)^2\right]\ln\left(\frac{2G}{\pi\sigma_Y}\right)}{C\,\sigma^2}\right\}^{1/2} . \qquad (12)$$

It was initially assumed that cracking would propagate through the weakest part of a material, and in a bainitic steel such

(534)

as steel armor this would be in the ferrite. With this assumption and the properties of ferrite, which cleaves on {100} planes, it was estimated with Eq. 12 that the radius of the crack nucleus activated with an applied stress of 1.65 GPa should be 3.9μm in 1.27cm thick RHA plate. A radius of 1.3μm is predicted for a 2.88 GPa load. This is in approximate agreement with the smallest cracks that have been observed, but the crack velocity computed with the same assumptions was found to be greater than has been observed.

The possibility that cracks might pass the strongest barriers was tested by expressing γ in terms of the fracture toughness of RHA. At an applied stress of 2.88 GPa, this procedure predicted a nucleus radius of 0.019cm. This is larger than most of the observed cracks as documented in Fig. 1. The conclusion from this must be that for stresses up to at least 2.88 GPa cracks do not propagate straight through rolled steel armor without regard for the microstructure.

The results for the two conditions investigated above indicate that initial crack growth is in the ferrite since the critical nucleus size computed is about the size of the smallest cracks observed, but these cracks must stop when they intersect strong barriers. This is why the average crack velocity is less than computed. The computed velocity applies only up to the time the crack is stopped. Continued growth can be by either coalescence of cracks or reactivation of the stopped crack. If continuation were by coalescence, there should be a sea of microcracks surrounding the main crack. There is some evidence of this where there are clusters of inclusions, but this is not typical. Continued growth by reactivation is the alternative. Irregular continuous cracks should be expected when barriers are important and overcome by reactivation of a stopped crack, for if barriers are important, the crack will continue to propagate in the weakest phase. Hence, it will change direction as it moves into material with a different crystallographic orientation. An irregular crack path is exactly what is seen in Fig. 3. Why is a delay time required if the applied stress is greater than the nucleation threshold stress σ_{no}? It is proposed that this time is required for the crack to open sufficiently to activate the blunted crack at the barrier.

At this point, several features of the breaking process have been clarified, but it is apparent that $\dot{C}_p$ cannot be equated to $\dot{R}$ for all C to establish fracture parameters because crack growth is intermittent.

Presumably, Eq. 12 gives the correct crack velocities when growth is in progress, but part of the time the cracks are blocked.

5-35

The effective velocity is given by

$$\dot{C}(C)_E = \frac{l_i \cos\theta_i}{\Delta t_{ci} + \Delta t_{oi}} = \frac{\dot{C}_p(C)\ \Delta t_{ci} \cos\theta_i}{\Delta t_{ci} + \Delta t_{oi}}, \qquad (13)$$

where the subscript i identifies the segment of the crack to open as the crack grows from C to C+ΔC, l_i is the length of the crack segment breaking, $\cos\theta_i$ is the projection of l_i onto the main crack path, Δt_{ci} is the time during which the crack propagates and Δt_{oi} is the time during which the crack is blocked at a barrier before cracking starts along l_i. As the crack lengthens, segments break more quickly according to Eq. 12, which means Δt_{ci} decreases with C. The dwell time at barriers should also decrease since the time to attain the crack opening sufficient to overcome a barrier must decrease as the rate at which the crack opens increases. It is proposed that the dependence of Δt_{oi} on C is approximated by letting Δt_{oi} be proportional to Δt_{ci}. Then $\Delta t_{oi} = F\Delta t_{ci}$, and

$$\dot{C}(C)_E = \dot{C}_p \cos\theta_i/(1+F). \qquad (14)$$

As indicated in §III, cracks nucleate in RHA at inclusions and grow in the weak bands of the microstructure, but the MnS inclusions are concentrated in the weak bands. This leads to the coalescence of major coplanar cracks after growth dependent on the inclusion spacing. Since the parameters listed in Table I were determined to represent the intermediate stage of cracking, $\dot{R}$ computed with these parameters and Eq. 3 should reflect crack growth and coalescence except for crack lengths less than the inclusion spacing. Then, $\dot{R}$ equals $\dot{C}_E$. This equality at sufficiently small crack sizes allows $\cos\theta_i/(1\mp F)$ to be determined from experimental measurements for an average angle θ_i characteristic of the steel. Now, Eqs. 12 and 14 should reasonably express the magnitude and material dependence of the crack velocity in sound material.

Eq. 12 is based on the plastic work at the new surface created as a crack propagates and on the effect of plastic deformation on the stress field bounding the crack tip. Hence, the form of the equation and the yield strength, which is included in the result, reflect the plastic nature of the material. Although nucleation and growth have been related to the banding and inclusions of steel armor, the quantitative effects of these microstructural features on $\dot{C}_E$ are not explicitly stated, and as far as the author knows, they have escaped previous description. However, one effect of the inclusions on the crack velocity is now apparent. They limit the maximum crack length on which the crack velocity is directly dependent. The crack

(531)

length is bounded because the MnS inclusions exist in planes of the banded microstructure and because cracks are nucleated at the inclusions independently, as described in §II. The maximum crack length is approximately half the inclusion spacing since coalescence must occur when the cracks reach this length. The width and spacing of the bands of the microstructure, in which the sulfides occur, establishes the actual inclusion spacing for a given sulfide volume and inclusion size. In this way, the banding of the steel indirectly affects the crack velocity.

The new point stressed is that quantitative predictions of the crack velocity of steel armor can be made with Eqs. 12 and 14 as a function of the chemistry and processing of the steel. This is possible because the spacing and width of the bands in which the MnS inclusions reside, the sulfur content of the steel and the inclusion size establishes the distance between the inclusions and the crack length on which the crack velocity is directly dependent.

Manufacturing techniques allow substantial control over the sulfide inclusions in a steel. For example, by varying the sulfur content from 10^2 to 10^4 ppm and the inclusion diameter from 0.1 to 10μm, the distance between inclusions can be changed from 0.2 to 200μm. This is equivalent to limiting the maximum crack size and, therefore, the crack velocity.

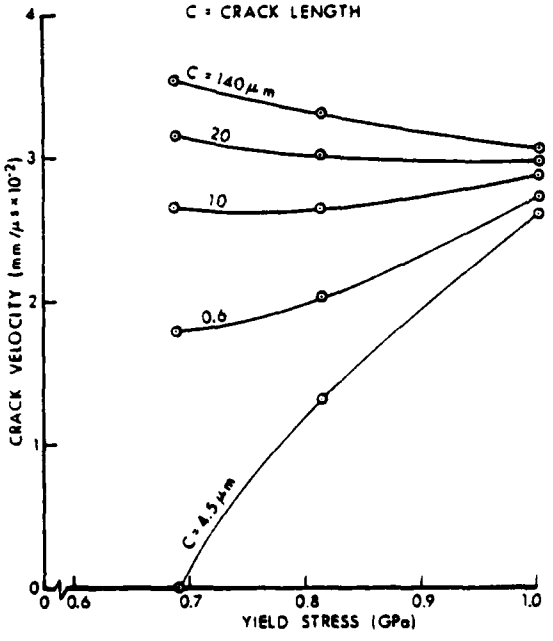

Figure 5. Crack Velocity under an applied stress of 2.88 GPa.

The effect of the crack size and the yield strength on the crack velocity predicted with Eq. 14 is illustrated in Fig. 5 for an applied stress of 2.88 GPa. It is apparent that the crack velocity can either increase or decrease as the yield strength is decreased. Whichever occurs, depends on the crack size. This is a new result that occurs because of the effect of the plastic zone on the stress field at the crack tip.

637

When cracks are long, it is clear that the crack velocity increases to infinity as σ_Y goes to zero. This occurs because ρ_t is proportional to σ_Y^{-1}, but there is a degree of realism to the result. It can be interpreted as though the entire cross section of the sample is the process zone of a crack with complete certainty that microcracking will occur everywhere in this zone.

The material parameter N_o is the total number of crack nuclei. The total number available equals the number of inclusions larger than the critical nucleus size. The parameter $\dot{N}_o$ is the nucleation rate when σ equals σ_{no}. This should be proportional to the density of available nucleation sites and, therefore, to the inclusion density. Hence, $\dot{N}_o = KN$. The proportionality constant was estimated with results from the program in which the parameters in Table I were determined. The parameter N_o and the relation for $\dot{N}_o$ are two quantitative ways of expressing the effects of inclusions on spallation.

Methods of predicting the void nucleation threshold stress σ_{no} have been proposed, but in each of these, the shape of the void must be known, or assumed. Bounds can be placed on σ_{no} as a function of the yield strength, but these allow widely different values of σ_{no} for a given yield stress. At this point, an experimental determination of the dependence of σ_{no} on the yield strength is more reliable. Such observations for steel armor reveal that in the yield strength range from $0.75 \leqq \sigma_Y \leqq 1.0$ GPa, σ_{no} increases as σ_Y decreases. These experimental results were used in the material computations described next.

V. ARMOR DESIGN

A new method of designing a material to resist spallation is proposed that is based on the crack nucleation and growth-rate equations, the dependence of these equations on the governing material properties and a method of computing the damage for a given impulse. In such a design, the anticipated stress history is an important design condition. Stresses can be applied that will certainly eventually destroy an armor plate. The general question is, How resistant is a material to a stress for a specific time? The design and performance of a material are closely tied to the impulse it must withstand.

The rate equations and the governing material properties have been described, but these are not sufficient to fully assess the changes in spallation resistance with material changes. A description is still required of the in-plane crack coalescence that is related to the planar arrays of MnS inclusions. The inclusion spacing governs

3.38

this coalescense rate directly, and it is a major effect of the inclusions since coalescence is an especially abrupt unzipping mechanism by which a material comes apart. The approach taken here was to selectively treat the damage of the weak bands of the banded microstructure, which is where failure actually occurs, rather than to assume uniformly distributed damage. Coalescence was computed with a random linear coalescence model(10) in which a new crack is created whenever two cracks collide. The new crack length is the sum of the lengths of the colliding cracks, and the number of cracks is reduced by one each time there is a collision. Damage was computed with this model by determining the fraction f of a sample covered by cracks. The smaller f, the more resistant a material is to spallation.

Average crack velocities were estimated with Eq. 14 and a crack length limited by half the inclusion spacing which was specified as part of the material design.

The result of these considerations is that the approximate effect of yield strength, band thickness, band separation and inclusion size and density on the nucleation, growth and coalescence of cracks and the damage of rolled steel armor can be computed. Hence, it is possible to design the spallation resistance of such a material as a function of the governing material variables. Computations to demonstrate this have been completed, and a representative result is shown in Fig. 6.

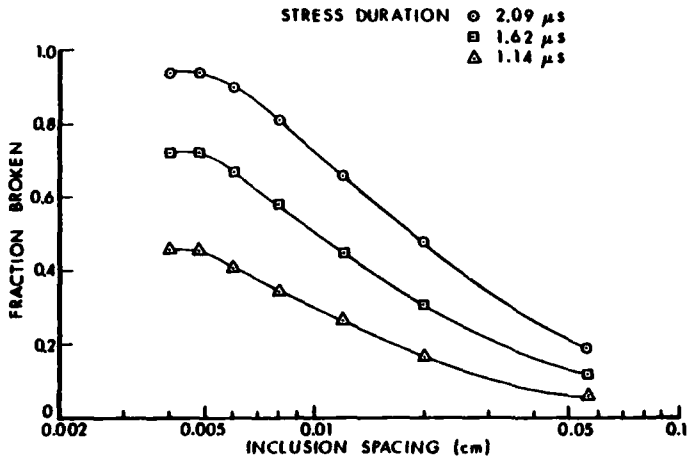

Figure 6. Extent of failure created with stress waves.

Results from this approach to material design should allow quantitative material considerations that have been impossible in the past. The role of inclusions and banding are specific examples. Furthermore, it should allow many new types of decisions to be made about material selection prior to expensive procurements and field

539

tests. For example, it may be possible to select material conditions to allow a prespecified degree of damage.

New conclusions about the role of inclusions can also be derived from Fig. 6. It appears that for the loads considered an inclusion spacing of from 40 to 50μm is particularly undesirable. It is noted that cleaning a material moderately, i.e., increasing the inclusion spacing from 40 to 60μm does not improve the spallation resistance much. Finally, there is an inclusion spacing beyond which the effect of cleaning the material becomes less pronounced.

VI. CONCLUSIONS

a. Crack nucleation occurs at inclusions in rolled steel, and cracks propagate in the weak bands of the banded microstructure.

b. A comparison of the microstructural details of fracture in rolled steel with the cumulative crack-size distribution reveals that planar crack coalescence accompanies an intermediate stage of failure. Crack velocities determined for this stage of cracking without regard for coalescence do not represent true crack velocities.

c. Late stage coalescence of non-coplanar cracks occurs by plastic shear on connecting surfaces.

d. The method proposed for material design to resist spallation can be successfully applied when the governing material characteristics can be related to the crack nucleation and growth-rate equations. The inclusion spacing, banded microstructure and flow stress of rolled steel relate to these rate equations. Hence, material design considerations are possible for rolled steel.

e. Minor increases in inclusion spacing may not improve spallation resistance appreciably. There is an inclusion spacing beyond which only small gains in spallation resistance are possible.

VII. ACKNOWLEDGEMENT

It is a pleasure to acknowledge helpful technical discussions with Dr. Donald Curran in which he indicated he had independently concluded that cracks must propagate intermittently under certain conditions.

(540)

REFERENCES

1. G. Moss and C. M. Glass, "Some Microscopic Observations of Cracks Developed in Metals by Very Intense Stress Waves," Ballistic Research Laboratories Technical Note No. 1312, April 1960.

2. C. M. Glass, G. L. Moss, and S. K. Golaski, "Effects of Explosive Loading on Single Crystals and Polycrystalline Aggregates," Response of Metals to High Velocity Deformation, Ed. Shewman and Zackay, Interscience Publishers, New York, 1961, pp. 115-143.

3. T. Barbee, L. Seaman, and R. C. Crewdson, "Dynamic Fracture Criteria of Homogeneous Materials," Technical Report No. AFWL-TR-70-99, Air Force Weapons Laboratory, Kirtland Air Force Base, New Mexico, Nov. 1970.

4. T. W. Barbee, Jr., L. Seaman, R. Crewdson, and D. Curran, "Dynamic Fracture Criteria for Ductile and Brittle Metals," J. Materials, Vol. 7, No. 3, 1972, pp. 393-401.

5. Lynn Seaman, Donald R. Curran, and Donald A. Shockey, "Computational Models for Ductile and Brittle Fracture," J. Appl. Phys., Vol. 47, 11, 1976, pp. 4814-4826.

6. L. Seaman, T. W. Barbee, Jr., and D. R. Curran, Technical Report No. AFWL-TR-71-156, Air Force Weapons Laboratory, Kirtland Air Force Base, New Mexico, Feb., 1972.

7. B. L. Averbach, D. K. Felbeck, G. T. Hahn, and D. A. Thomas, Fracture, John Wiley & Sons, Inc., New York, 1959.

8. A. S. Tetelman and A. J. McEvily, Jr., Fracture of Structural Materials, John Wiley & Sons, Inc., New York, 1967, p. 296.

9. Frank A. McClintock, "On the Plasticity of the Growth of Fatigue Cracks," Fracture of Solids, Ed. Drucker and Gilman, Interscience Publishers, John Wiley & Sons, New York, 1963, pp. 65-102.

10. W. deRosset, "Coalescence of Cavities During Dynamic Fracture," BRL R 1631, Ballistic Research Laboratory, Aberdeen Proving Ground, MD., 1973.

541